Dissipative Particle Dynamics Simulation of Flow in Periodically Grooved Three-Dimensional Nano- and Micro-channels

Dorothea KASITEROPOULOU, Theodoros E. KARAKASIDIS *, Antonios LIAKOPOULOS *

* Corresponding author: Tel.: ++30 2421074163; Email: thkarak@uth.gr, Tel.: ++30 2421074111; Email: aliakop@uth.gr,
Hydromechanics and Environmental Engineering Laboratory, University of Thessaly, 38334, Pedion Areos, Volos, Greece

Abstract
Nonequillibrium flow in three-dimensional grooved nano- and micro-channels is investigated using the Dissipative Particle Dynamics simulation method. Roughness is introduced by periodically placing rectangular protruding elements on the upper channel wall. The protrusion length and height are varied and their effect on the flow is examined. The computed macroscopic quantities of practical interest include density, velocity, pressure, and temperature profiles as well as relations between the friction factor and the Reynolds number. When compared to the smooth channel case, lower flow velocities are observed in the central part of the channel for all cases studied. This reduction of velocities becomes more pronounced as the protrusion height increases. For the micro-channel, density, pressure and temperature remain almost constant in the central part of the channel and their pattern near and inside the cavities depend on the protrusion shape. In the nanochannel case, lower temperatures and pressures are observed for all grooved channels relative to the smooth channel case. For all channel cases studied the calculated friction factor decreases as Reynolds number increases, following a power law relation.

Keywords: Micro-flow, Nano-flow, grooved channel, Dissipative Particle Dynamics Simulation, Friction factor.

1. Introduction

During the last decades research effort has been made in order to model fluid flow over solid grooved surfaces. Their interest can be explained by the use of these surfaces in constructing recently developed Micro and Nano Electromechanical Systems (known as MEMS/NEMS).

In nanofluidics, Jabbarzadeh et al. (2000) investigated the effect of wall roughness characteristics and the molecular length of the lubricating fluid in a flow of liquid hexadecane in sinusoidal wall channels and found that larger roughness amplitudes result in a decrease of the slip and also that with shorter molecules the amount of slip is dramatically lower. Kim and Darve (2006) studied electro-osmotic flow of water molecules through nanochannels with different types of surface roughness and found that flow rate decreases as the period of surface roughness decreases and the amplitude increases. Priezjev and Troian (2006) investigated the behavior of a Newtonian liquid in steady planar flow and found that as the substrate wavelength approaches length scales comparable with the liquid molecular diameter, the continuum solutions overestimate the degree of slip. Yang (2006) investigated the surface roughness effect on the nanorheology and fluid slip of simple fluids in hydrophobic and hydrophilic nanochannels and found that no-slip or negative slip is observed at the interface due to the increase of drag resistance. Cao et al. (2006) investigated the fluid wetting and flow in nanochannels with grooved surfaces structured by nanoscale triangular modules and found that the nanostructures can be used to control the boundary slip and the friction of the liquid nanoflow. Actually, for a hydrophilic liquid-solid interface they enhance the hydrophilicity and they increase the hydrophobicity for a hydrophobic interface. Sofos et al. (2009) investigated the effect of

periodic wall roughness on the flow of liquid argon through krypton nanochannels and observed that the presence of the protruding elements lead to a reduction of the velocity values inside the cavities, as well as a reduction of the slip length near the rough wall. In microfluidics, Wang et al. (2003) studied the mixing effect in microchannels due to the presence of grooved surfaces and found that the asymmetric arrangement of grooves result in different mechanism to enhance mixing by create helical shaped recirculation of fluids. Yang and Fang (2005) investigated the effect of surface roughness on slip flows in hydrophilic and hydrophobic microchannels and found that the slip presents a power law dependence on the shear rate for the cases of hydrophilic surfaces while for the hydrophobic cases it increases linearly with shear rate for all grooved channels. Lin (2008) designed a micromixer composed of a channel with patterned grooves on the bottom and side of the channel. The proposed micromixer was designed to enhance the transverse rotation of the fluid in the microchannel. Cao et al. (2009) focused on molecular momentum transport at fluid-solid interfaces affected by various physical factors among them the surface roughness. They mention that a hydrophobic fluid-wall interaction in combination with rough elements could indeed enhance the velocity slip due to lotus effect.

Work has also been reported on experimental investigations. Greiner (1990) investigated the water flow through ducts with periodically grooved elements located into one wall. He found that while the absolute level of transport depends on the thermal and geometric conditions, the enhancement gained from 20% flow rate modulation is fairly insensitive to them. Herman and Kang (2002) visualized the unsteady temperature fields in a grooved channel with curved vanes using interferometry and found a heat transfer enhance by a factor of 1.5-3.5, when compared to the basic grooved channel, mainly due to increased flow velocities in the groove region. Stroock et al. (2002) investigated steady pressure-driven flows in microchannels at low Reynolds number, and found that the hydrodynamic dispersion along the channel is reduced relative to the channel with flat walls.

In the present work we study the flow in a nanochannel and microchannel and seek further insight into the effects of wall roughness on the flow macroscopic quantities based on the mesoscopic Dissipative Particle Dynamics method. Roughness is introduced by periodically placing rectangular protruding elements on one of the two channel walls. Pressure, density, velocity and temperature profiles are calculated for different groove shape. Friction factor versus Reynolds number is also presented.

The novelty of this work is the investigation of the roughness effect in a planar nanochannel and microchannel flow with a mesoscopic method and also the modification of the effect of wall roughness in the amplitude of friction factor, which is usually calculated for macroscopic flows. Knowledge of the amplitude of the friction factor in each case could be helpful in the design of nano- and micro-devices.

The paper is set up as follows. In section 2 the simulation method is presented. Results are shown and discussed in section 3, while section 4 contains concluding remarks.

2. Simulation Method

2.1. Channel Geometry and Modelling

We study the flow between two stationary parallel solid plates (see Fig.1). The lower wall is flat while the upper wall is rough characterized by periodically placed rectangular protruding elements. We considered roughness of three different lengths: $l_{ro}=0l_{tot}$, $l_{r1}=0.5l_{tot}$, $l_{r2}=0.25l_{tot}$ (case $l_{ro}=0l_{tot}$ is the smooth channel, case $l_{r1}=0.5l_{tot}$ corresponds to one rectangular groove in the computational domain, $l_{r2}=0.25l_{tot}$ to two rectangular grooves) and four different heights (h=0.10H, h=0.20H, h=0.30H, h=0.40H, where H represents the height of the computational domain along the y-direction). Baseline dimensions of all computational domains in x-, y- and z-directions are L_x x L_y x L_z = 1.11 μm x 1.3μm x 1.1 μm for the micro- and 3.77nm x 4.72nm x 3.77nm for the nanochannel (in DPD units the dimensions are

L_x x L_y x L_z = 11.14 r_c x 13.00 r_c x 11.14 r_c and 11.09 r_c x 13.87 r_c x 11.09 r_c respectively, where r_c is the cut-off distance for all pairwise interactions). Conversion from DPD units to real units is discussed in detail in Kumar et al. (2009).

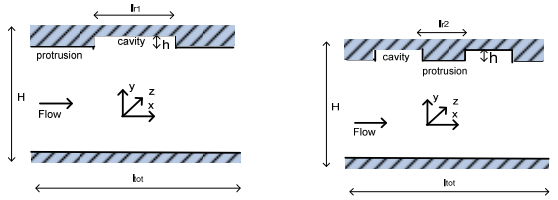

Figure 1: Schematics of computational domains.

2.2. Mathematical Model and Computational Details

The DPD system consists of N particles. For the i-th particle we denote mass m_i, position $\vec{r}_i$ and velocity $\vec{\upsilon}_i$, i=1,2,…N. For a single-component DPD liquid the forces exerted on a particle i due to particle j consists of three terms: 1) the conservative force $\vec{F}_{ij}^{\,C}$, 2) the dissipative force $\vec{F}_{ij}^{\,D}$ and 3) a random force $\vec{F}_{ij}^{\,R}$, given by,

$$\vec{F}_{ij}^{\,C}\left(r_{ij}\right)=\begin{cases}\alpha_{ij}\left(1-r_{ij}/r_c\right)\hat{r}_{ij}, & r_{ij}\le r_c\\ 0, & r_{ij}>r_c\end{cases} \quad (1)$$

$$\vec{F}_{ij}^{\,D}=-\gamma\omega^D(r_{ij})(\vec{\upsilon}_{ij}\cdot\hat{r}_{ij})\hat{r}_{ij} \quad (2)$$

$$\vec{F}_{ij}^{\,R}=\sigma\omega^R(r_{ij})\xi_{ij}\hat{r}_{ij} \quad (3)$$

where $\vec{r}_{ij}=\vec{r}_i-\vec{r}_j$, $r_{ij}=\left|\vec{r}_{ij}\right|$, $\hat{r}_{ij}=\dfrac{\vec{r}_{ij}}{\left|\vec{r}_{ij}\right|}$, $\vec{\upsilon}_{ij}=\vec{\upsilon}_i-\vec{\upsilon}_j$ (Keaveny et al. 2005) and α_{ij} is the maximum repulsion between particles i and j (Groot and Warren 1997). The coefficients γ and σ determine the amplitude of the dissipative and random forces, respectively, while ω^D and ω^R are appropriate weight functions (Fedosov et al. 2008). The weight functions ω^D and ω^R provide the range of interaction for the dissipative and random forces (Espanol and Warren 1995). In Eq (3), ξ_{ij} is a random variable with Gaussian statistics (Groot and Warren 1997). By enforcing $\xi_{ij}=\xi_{ji}$ one satisfies the principle of momentum conservation (Karniadakis et al. 2002). All the forces between particle i and j vanish beyond a cut-off radius r_c (Trofimov 2003). The random force coefficient, σ, and the system temperature are the same for all cases studied here and their value was chosen following the methodology proposed by Groot and Warren (1997).

The requirement of canonical distribution sets two conditions linking the random and dissipative forces. The first one couples the weight functions through

$$\omega^D\left(r_{ij}\right)=\left[\omega^R\left(r_{ij}\right)\right]^2 \quad (4)$$

and the second one the strengths of the random and dissipative forces via

$$\sigma^2=2\gamma k_BT \quad (5)$$

where k_B is the Boltzmann constant (Nikunen et al. 2003). The typical choice for the weight functions is

$$\omega^R\left(r_{ij}\right)=\begin{cases}\left(1-r_{ij}/r_c\right)^p, & for\ \ r_{ij}\le r_c\\ 0, & for\ \ r_{ij}>r_c\end{cases} \quad (6)$$

where $p=1$, for the standard DPD method (Fedosov et al. 2008).

The time evolution of velocities and positions of particles is described by Newton's second law of motion written in the form (Pivkin and Karniadakis 2005)

$$d\vec{r}_i=\vec{\upsilon}_i dt \quad (7)$$

$$d\vec{\upsilon}_i=\frac{1}{m}\left(\vec{F}_i^{\,C}dt+\vec{F}_i^{\,D}dt+\vec{F}_i^{\,R}\sqrt{dt}\right) \quad (8)$$

where $\vec{F}_i^{\,C}=\sum_{i\neq j}\vec{F}_{ij}^{\,C}$, $\vec{F}_i^{\,D}=\sum_{i\neq j}\vec{F}_{ij}^{\,D}$ and $\vec{F}_i^{\,R}=\sum_{i\neq j}\vec{F}_{ij}^{\,R}$.

All simulations are conducted with the open source LAMMPS package (Plimpton 1995). The number density of the DPD fluid, n_f, is equal to 3 for the nanochannel and 10 for the microchannel, while the random and dissipative forces, σ and γ respectively are set equal to those described in Pivkin and Karniadakis (2005).The conservative force parameter, α_{ij} is equal to 25 for the

nanochannel and 7.5 for the microchannel. System temperature is kept constant at T*=1. The investigation of these parameters for a planar flow in the nanochannel case is described in Kasiteropoulou et al. (2011a).

Periodic boundary conditions are employed along x- and z-directions. Bounce-back conditions are enforced in order to avoid that fluid particles cross the wall, since the effective forces are not sufficient to prevent wall penetration (Revenga et al. 1999; Pivkin and Karniadakis 2005). In bounce-back conditions whenever a fluid particle is found within a given distance from the wall, it is reflected back into the fluid to the symmetric position about the wall surface. The sign of the velocity of the particle in the direction normal to the wall is also reversed (Zhigang and Drazer 2008). Wall particles are bound on simple cubic sites and their velocities are set equal to zero.

Along the x-direction four values of external driving force F_{ext}= 0.01, 0.02, 0.03 and 0.04 (in DPD units) are applied to each particle to drive the flow. The Reynolds number is defined as $\mathrm{Re} = \mathrm{Re}_{D_h} == \frac{\overline{\upsilon}(D_h)}{\nu} = \frac{\overline{\upsilon}(2\overline{h})}{\nu}$, where $\overline{\upsilon}$ is the mean velocity of the fluid, D_h is the hydraulic diameter, $\overline{h}$ is the distance between the two parallel solid plates and ν is the kinematic viscosity of the fluid as described in Groot and Warren (1997). The friction factor is defined as $f = \frac{(2\overline{h})F_{ext}}{0.5m\overline{\upsilon}^2}$.

The simulation step for the system is $\Delta t = 0.01\sqrt{mr_c^2/k_BT}$ (0.015ps for the nanochannel and 7.6×10^{-3}μs for the microchannel in physical units). The duration of the simulation is 5×10^5 time steps. Pressure, number density, temperature and streaming velocity bin values are averaged over the last 2.5×10^5 time steps of the simulation.

2.3. Post Processing

Local pressure, number density, temperature and streaming velocity values are calculated at parallelepiped bins. Results presented in this work are obtained by dividing the computational domain into 4x80x80, 8x80x80 or 16x80x80 bins along the direction x, y, z respectively for post processing.

Pressure values are obtained from the trace of the stress tensor

$$p = -\frac{1}{3}tr\mathbf{S} \qquad (9)$$

where the stress tensor, $\mathbf{S}$, is calculated using the Irving– Kirkwood theory (Irving and Kirkwood 1950; Fan et al. 2003):

$$\mathrm{S} = -\frac{1}{\mathrm{V}}\left[\mathrm{m}\sum_{\mathrm{i}}(\vec{\upsilon}_{\mathrm{i}} - \vec{\upsilon}\ )(\vec{\upsilon}_{\mathrm{i}} - \vec{\upsilon}\ ) + \frac{1}{2}\sum_{\mathrm{i}}\sum_{\mathrm{j}\neq\mathrm{i}}\vec{\mathrm{r}}_{\mathrm{ij}}\vec{\mathrm{F}}_{\mathrm{ij}}\right] \qquad (10)$$

Here V is the volume of the computational bin, $\vec{\upsilon}$ is the corresponding stream velocity and $\vec{F}_{ij}$ is the interparticle force on particle i due to particle j:

$$\vec{F}_{ij} = \vec{F}_{ij}^{\,C} + \vec{F}_{ij}^{\,D} + \vec{F}_{ij}^{\,R} \qquad (11)$$

Temperature is calculated in each bin across the channel using the equation

$$T = \frac{m}{3Nk_B}\sum_{i=1}^{N}\left(\vec{\upsilon}_i - \vec{\upsilon}\ \right)^2 \qquad (12)$$

where N is the number of particles inside the bin.

3. Results

3.1. Macroscopic quantity profiles

Number density profiles at the protrusion and the cavity midplanes are presented in Fig. 2. Fluid particle localization is similar for the nanochannel and the microchannel case with peaks located at a distance from the walls ($0.87r_c$ and $0.44r_c$ for the nanochannel and the microchannel case respectively). For the nanochannel case, at the protrusion midplanes density is homogeneous and slightly lower than its average value in the core of the channel while at the cavity midplanes is slightly higher. In the microchannel case, at the protrusion midplanes density is almost equal to its average value in the core of the channel within statistical errors, while at the cavity midplanes density is lower. It should be also noted that in the microchannel case a high density peak is detected in the density profile

very close to the protrusion surface (y≈1.40 for h=0.30H). Inside the cavities high number density regions are detected for both channel scales and suggest the possibility of particle trapping in these regions. Particle trapping is confirmed by computing the particle residence time and by the analysis of particle trajectories and is discussed in detail in Kasiteropoulou et al. (2011b) (nanochannel) and in Kasiteropoulou et al. (2011c) (microchannel).

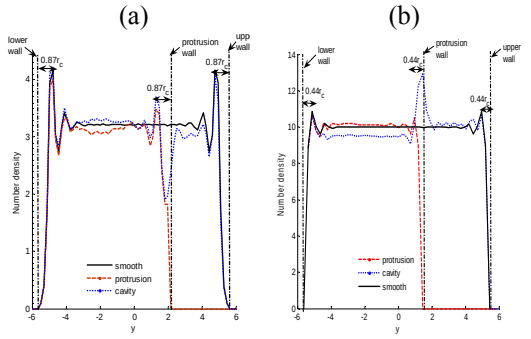

Fig. 2. Local number density profiles at the protrusion midplanes and the cavity midplanes for Fext=0.04, lr2=0. 25ltot and h=0.30H. a) Nanochannel and b) Microchannel (y is in r_c units). Dash-dot lines denote solid wall limits.

Bin averaged velocity profiles are presented in Fig.3 for a typical nanochannel and microchannel case. It turns out that the average velocity is systematically reduced as the protrusion height increases for all channel cases investigated in this work.

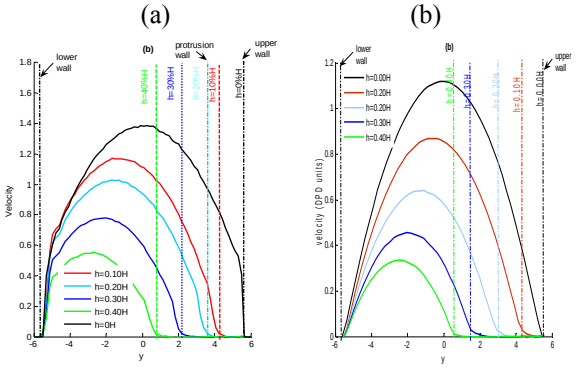

Fig. 3. Bin-averaged velocity profiles over the whole channel region for Fext=0.02 and lr2=0.25ltot. a) Nanochannel and b) Microchannel (y is in r_c units). Dash-dot lines denote solid wall limits.

Interesting characteristics are presented in Fig.4 where a comparison between DPD and Stokes results is performed for protrusion length lr1=0.5ltot and protrusion height h=0.20H. We observe that local velocity profiles are in good agreement at the protrusion midplanes, and at the cavity midplanes Stokes overestimate the velocities inside the cavities. Similar behavior is observed for protrusion length lr1=0.5ltot and protrusion height h=0.10H and is discussed in Kasiteropoulou et al. (2011b).

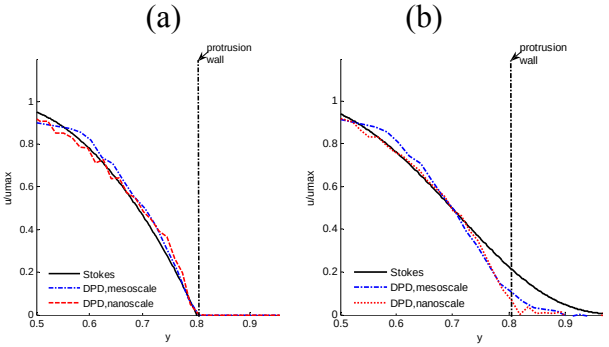

Fig. 4. Local velocity profiles at the protrusion midplane and the cavity midpplane for case $l_{r1}=0.5l_{tot}$ and h=0.20H. Comparison between DPD and Navier-Stokes solutionσ at Re≈15. a) Protrusion and b) Cavity. Vertical dash-dot lines denote solid wall limits.

Pressure behaviour also reveals interesting characteristics (Fig.5). Both in nanochannel and microchannel case, pressure remains constant in the central part of the channel and decreases as we move towards to the walls.

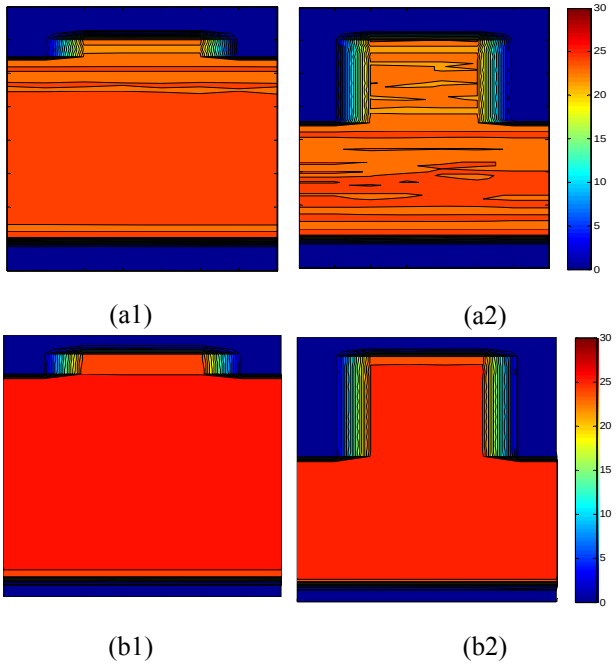

Fig. 5. Isobars for a) Nanochannel and b) Microchannel for cases 1) lr1=0. 50ltot and h=0.10H and 2) lr1=0. 50ltot and h=0.40H. Fext = 0.02 DPD units.

This reduction is more pronounced as the external driving force increases for all channel cases. High pressure regions are observed inside the grooves and their magnitude depends on the groove shape (Figs. 5b1, 5b2). The average maximum pressure value and the pressure inside the cavities depend both on the protrusion length and height. Smaller protrusion lengths and higher protrusion heights lead to pressure reduction.

Isotherms for typical channel cases are presented in Fig. 6. In nanochannel case, temperature values in the core of the channel for all grooved channels are lower relative to the initial temperature of the system (see section 2.2: T*=1). This reduction depends only on the protrusion length and actually temperature decreases as the protrusion length decreases (Fig.6 a2). Keeping the protrusion length constant the protrusion height doesn't seem to affect the temperature map. In microfluidics, temperature map reveal differences relative to the nanochannel case. Temperature values in the core of the channel are the same with the initial one independent on the protrusion shape.

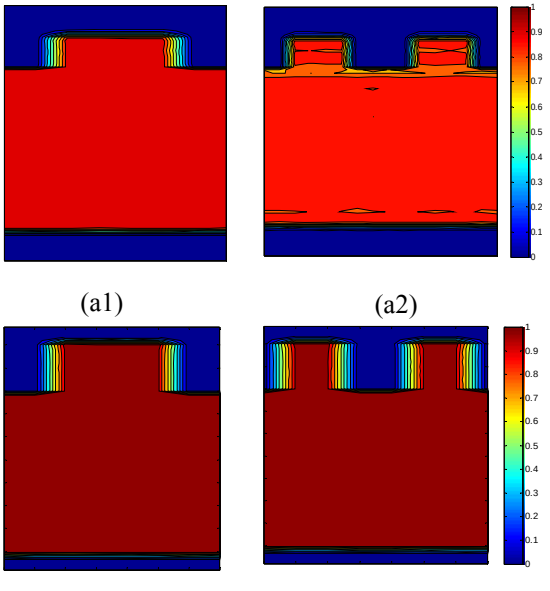

(a1) (a2)

(b1) (b2)

Fig. 6. Isotherms for a) Nanochannel and b) Microchannel for cases 1) lr1=0. 50ltot and h=0.10H and 2) lr1=0. 50ltot and h=0.40H. Fext = 0.02 DPD units.

3.2. Friction factor versus Reynolds number relations

The calculated friction factor versus Reynolds number diagram is compared with theoretical relations for planar Poiseuille flow. For all channel cases the friction factor decreases as Reynolds number increases, following a power law relation (representative results are presented in Fig. 7). This behavior is more pronounced as the protrusion length decreases and the protrusion height increases. The model predicts fRe=constant in the range 20≤Re≤100 and its value depend on the protrusion size (see Table1).

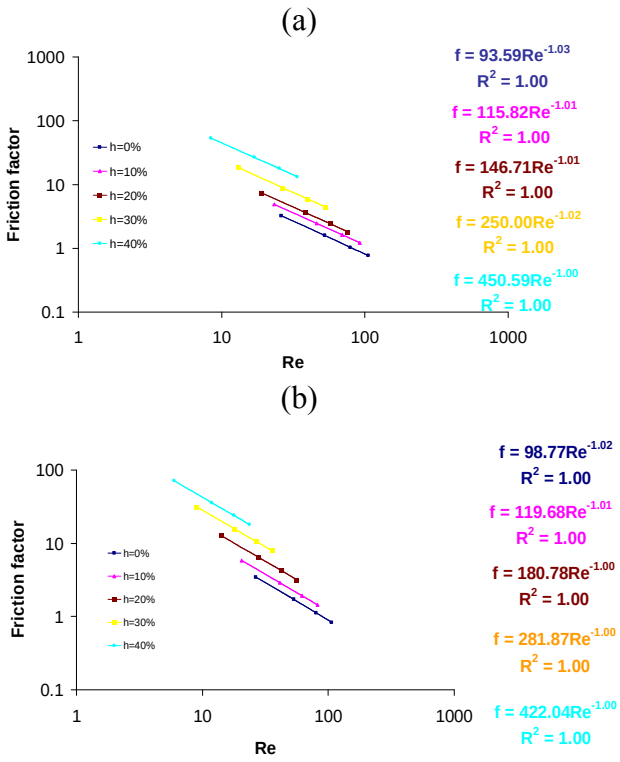

Fig. 7. Friction factor versus Reynolds number for all protrusion heights and Fext values. Protrusion length is equal to lr2=0.25ltot. a) Nanochannel and b) Microchannel.

Protrusion length, l_{ri} / Protrusion height, h	l_{r1}=0.50l_{tot}	l_{r2}=0. 25l_{tot}
0.10H	**118.52 (a)** 110.54 (b)	**119.68 (a)** 115.82 (b)
0.20H	**180.61 (a)** 126.58 (b)	**180.78 (a)** 146.71 (b)
0.30H	**278.14 (a)** 214.96 (b)	**281.87 (a)** 250.00 (b)
0.40H	**409.48 (a)** 374.39 (b)	**422.04 (a)** 450.59 (b)

Table 1: Values of Poiseuille number fRe = A = constant for each protrusion size studied (a) microchannel, (b) nanochannel.

The increase of the friction factor value due to the presence of the rectangular protruding elements has also been quantified for flow in macrochannels (Kasiteropoulou 2011c). The macro-flow has been studied by solving the Navier-Stokes equation for protrusion length equal to l_{r1} and protrusion heights 0.10H and 0.20H (see Table 2).

Protrusion size / **Channel scale**	$\mathbf{l_{r0}=0l_{tot}}$ **h =0H**	$\mathbf{l_{r1}=0.50l_{tot}}$ **h =0.10H**	$\mathbf{l_{r1}=0.50l_{tot}}$ **h =0.20H**
Nanochannel (DPD)	93.59	110.54	126.58
Microchannel (DPD)	98.77	118.52	180.61
Macrochannel (FE)	98.36 (96 theory)	107.20	153.40

Table 2: Values of Poiseuille number fRe = A = constant for nanochannel, microchannel, and macrochannel flows. (Kasiteropoulou et al., 2011b; Kasiteropoulou et al., 2011c)

4. Conclusions

Fluid particle localization is similar for the nanochannel and the microchannel case, as high density peaks are detected for both cases inside the cavities and near the solid walls. Differences are observed in the core of the channel and in the cavity and protrusion midplanes. In particular, in the nanochannel and the protrusion midplane density is slightly lower than its average value and at cavity is higher, in addition to the microchannel case where at the protrusion midplane it is equal to its average value and at the cavity it is lower. Density peaks inside the cavities reveal trapping of fluid inside the rectangular cavities. This particle trapping affects macroscopic quantities considered here such as velocity, pressure and temperature distribution inside and close to the cavities. Velocity reduces systematically and this reduction becomes more pronounced as the protrusion height increases. For the microchannel, the pressure and temperature remain almost constant in the core of the channel and their pattern near and inside the cavities depend on the protrusion shape. In the nanochannel case, lower temperatures and pressures are observed for all grooved channels relative to the smooth channel case.

The effect of wall roughness on the flow is significant and should be further investigated for various wall and fluid materials in combination with the protrusion shape. One has to take into consideration this effect in the design of nano- and micro-devices.

References

Cao, B.Y., Chen, M., Guo, Z.Y., 2006. Effect of Surface Roughness on Gas Flow in Microchannels by Molecular Dynamics Simulation, Int. J. Eng. Sci. 44, 927-937. doi:10.1016/j.ijengsci.2006.06.005

Cao, B.Y., Sun, J., Chen, M., Guo, Z.Y., 2009. Molecular Momentum Transport at Fluid Solid Interfaces in MEMS/NEMS: A Review, Int. J. Mol. Sci. 10, 4638-4706. doi: 10.3390/ijms10114638

Espanol, P., Warren, P., 1995. Statistical mechanics of dissipative particle dynamics, Europhys. Lett. 30, 191-196. doi: 10.1209/0295-5075/30/4/001

Fan, X., Phan-Thien, N., Yong, N., Wu, X., Xu, D., 2003. Microchannel flow of a macromolecular suspension, Phys. Fluids 15, 11-21. doi:10.1063/1.1522750

Fedosov, D.A., Pivkin, I.V., Karniadakis, G.E., 2008. Velocity limit in DPD simulations of wall-bounded flows, J. Comput. Phys. 227, 2540-2559. doi: 10.1016/j.jcp.2007.11.009

Greiner, M., 1990. An experimental investigation of resonant heat transfer enhancement in grooved channels, Int. J. Heat Mass Transfer 34(6), 1383-1391. doi:10.1016/0017-9310(91)90282-J

Groot, R.D., Warren, P.B., 1997. Dissipative particle dynamics: bridging the gap between atomistic and mesoscopic simulation, J. Chem. Phys. 107, 4423-4435.

Herman, C. and Kang, E., 2002. Heat transfer enhancement in a grooved channel with curved vanes, Int. J. Heat Mass Transfer 45, 3741-3757. doi:10.1016/S0017-9310(02)00092-3

Irving, J.H., Kirkwood, J.G., 1950. The statistical mechanics of transport processes. IV. The equation of hydrodynamics, J. Chem. Phys. 18, 817.

Jabbarzadeh, A., Atkinson, J. D., Tanner, R.I., 2000. Effect of the wall roughness on slip and rheological properties of hexadecane in molecular dynamics simulation of Couette shear flow between two sinusoidal walls, Phys. Rev. E 61, 690-699. doi:10.1103/PhysRevE.61.690.

Karniadakis, G., Beskok, A., Aluru, N., 2002. Microflows and Nanoflows: Fundamentals and Simulation. Springer, New York.

Kasiteropoulou, D., Karakasidis, T.E., Liakopoulos, A., 2011a. Dissipative Particle Dynamics investigation of parameters affecting planar nanochannel flows. Mater. Sci. Eng. B. doi: 10.1016/j.mseb.2011.01.023 (accepted for publication).

Kasiteropoulou, D., Karakasidis, T., Liakopoulos, A., 2011b. A Dissipative Particle Dynamics study of flow in periodically grooved nanochannels. Internat. J. Numer. Methods Fluids (accepted for publication).

Kasiteropoulou, D., Karakasidis, T., Liakopoulos, A., 2011c. Microfluidics simulations in periodically grooved channel by Dissipative Particle Dynamics. (submitted for publication).

Keaveny, E.E., Pivkin, I.V., Maxey, M., Karniadakis, G., 2005. A comparative study between dissipative particle dynamics and molecular dynamics for simple- and complex-geometry flows, J. Chem. Phys. 123, 104107-1-104107-9. doi: 10.1063/1.2018635

Kim, D., Darve, E., 2006. Molecular dynamics simulation of electro-osmotic flows in rough wall nanochannels, Phys. Rev. E 73, 051203:1-051203:12. doi: 10.1103/PhysRevE.73.051203

Kumar, A., Asako, Y., Abu-Nada, E., Krafczyk, M., Faghri, M., 2009. From dissipative particle dynamics scales to physical scales: a coarse-graining study for water flow in microchannel, Microfluidics and Nanofluidics 7, 467-477. doi: 10.1007/s10404-008-0398-x

Lin, W., 2008. A Passsive Grooved Micromixer Generating Enhanced Transverse Rotation for Microfluids, Chem. Eng. Technol. 31(8), 1210-1215. doi: 10.1002/ceat.200800091

Nikunen, P., Karttunen, M., Vattulainen, I., 2003. How would you integrate the equations of motion in dissipative particle dynamics simulations?, Comput. Phys. Commun. 153, 407-423. doi:10.1016/S0010-4655(03)00202-9

Pivkin, I.V., Karniadakis, G.E., 2005. A new method to impose no-slip boundary conditions in dissipative particle dynamics, J. Comput. Phys. 207, 114-128. doi:10.1016/j.jcp.2005.01.006

Plimpton, S.J., 1995. Fast Parallel Algorithms for Short-Range Molecular Dynamics, J. Comput. Phys. 117, 1-19. doi>10.1006/jcph.1995.1039

Priezjev, N.V. and Troian, S.M., 2006. Influence of periodic wall roughness on the slip behaviour at liquid/solid interfaces: molecular-scale simulations versus continuum predictions, J. Fluid Mech. 554, 25-46. doi:10.1017/S0022112006009086.

Revenga, M., Zuniga, I., Espanol, P., 1999. Boundary conditions in dissipative particle dynamics, Comput. Phys. Commun. 121–122, 309-311. doi: 10.1016/S0010-4655(99)00341-0

Sofos, F.D, Karakasidis, T.E., Liakopoulos, A., 2009. Effects of wall roughness on flow in nanochannels, Phys. Rev. E 79, 026305:1-026305:7. doi: 10.1103/PhysRevE.79.026305.

Stroock, A.D., Dertinger, S.K.W., Ajdari, A., Mezic, I., Stone, H.A., Whitesides, G.M., 2002. Chaotic Mixer for Microchannels, Science 295, 647-651. doi: 10.1126/science.1066238

Trofimov, Y., 2003. Thermodynamic consistency in dissipative particle dynamics. Technische Universiteit Eindhoven, Ph.D. Thesis.

Wang, H., Iovenitti, P., Harvey, E., Masood, S., 2003. Numerical investigation of mixing in microchannels with patterned grooves, J. Micromech. Microeng. 13, 801-808. doi: 10.1088/0960-1317/13/6/302

Yang, S.C. and Fang, L.B., 2005. Effect of surface roughness on slip flows in hydrophobic and hydrophilic microchannels by molecular dynamics simulation, Molecular Simulation 31: 14, 971—977.doi: 10.1080/08927020500423778.

Yang, S.C, 2006. Effects of surface roughness and interface wettability on nanoscale flow in a nanochannel, Microfluid Nanofluid 2, 501-511. doi: 10.1007/s10404-006-0096-5

Zhigang, L., Drazer, G., 2008. Hydrodynamic interactions in dissipative particle dynamics, Phys. Fluids 20, 103601-1-103601-8. doi: 10.1063/1.2980039